UNIVERSITY *of York*

This is a repository copy of *Gas temperature measurements in a pulsed, low-pressure inductively coupled plasma in oxygen*.

White Rose Research Online URL for this paper:
https://eprints.whiterose.ac.uk/157117/

Version: Published Version

Article:

Meehan, David, Niemi, Kari orcid.org/0000-0001-6134-1974 and Wagenaars, Erik orcid.org/0000-0002-5493-3434 (2020) Gas temperature measurements in a pulsed, low-pressure inductively coupled plasma in oxygen. Japanese Journal of Applied Physics. SHHB03. ISSN 1347-4065

White Rose
university consortium
Universities of Leeds, Sheffield & York

eprints@whiterose.ac.uk
https://eprints.whiterose.ac.uk/

The Japan Society
of Applied Physics

Gas temperature measurements in a pulsed, low-pressure inductively coupled plasma in oxygen

To cite this article: David N. Meehan *et al* 2020 *Jpn. J. Appl. Phys.* **59** SHHB03

View the article online for updates and enhancements.

REGULAR PAPER

Gas temperature measurements in a pulsed, low-pressure inductively coupled plasma in oxygen

David N. Meehan, Kari Niemi, and Erik Wagenaars[*] [ID]

York Plasma Institute, Department of Physics, University of York, York YO10 5DD, United Kingdom

[*]E-mail: erik.wagenaars@york.ac.uk

Optical emission spectroscopy (OES) of the magnetic dipole allowed $O_2(b^1\Sigma_g^+)$ to $O_2(X^3\Sigma_g^-)$ transition was investigated as a non-intrusive gas temperature diagnostic for E-mode and H-mode inductively coupled plasmas (ICP) in oxygen. It was compared to tunable diode laser absorption spectroscopy using Ar admixtures, and OES of the nitrogen Second Positive System with nitrogen admixtures. O_2 OES provided accurate results for the E-mode ICP, 400–600 K for powers of 100–300 W, but in H-mode the method was unsuitable probably because of excitation of $O_2(b^1\Sigma_g^+)$ by metastable atomic oxygen. Rotational temperatures were measured, using N_2 OES with N_2 admixtures, for pulsed operation of the ICP with a 30 ms pulse duration and 15% duty cycle. It took 1–3 ms before the steady-state rotational temperatures were achieved. In addition, a small variation of matching network settings affects the plasma ignition delay time by several ms. © 2020 The Japan Society of Applied Physics

1. Introduction

Low pressure oxygen plasmas find use in several industrial applications e.g. for etching or functionalisation of materials.[1] The gas temperature in such oxygen plasmas plays a key role in the plasma chemistry and therefore in optimization of these plasmas for specific applications.[2]

Well-established techniques for measuring the gas temperature, from Doppler broadening or as rotational temperature, in low-temperature plasmas include tunable diode laser absorption spectroscopy (TDLAS) on argon metastable atoms[3] and optical emission spectroscopy (OES) on the nitrogen band $N_2(C^3\Pi_u, \nu' = 0)$ to $N_2(B^3\Pi_g, \nu' = 0)$.[4] However, for pure oxygen plasmas both these methods require a gas admixture for diagnostic purposes, which can be a limiting factor. OES on the magnetic dipole transition between $O_2(b^1\Sigma_g^+, \nu' = 0)$ and $O_2(X^3\Sigma_g^-, \nu'' = 0)$[5,6] could overcome these limitations. Zyryanov et al. used the O_2 OES diagnostic to reliably measure gas temperatures in a dc glow discharge at $\sim$660–6600 Pa (5–50 Torr), using a high-resolution spectrometer.[5] Here, we investigate whether this technique can also be applied in an industrially relevant plasma; an inductively coupled plasma (ICP) at pressures of 20–50 Pa.[6] Measurements of the new O_2 OES diagnostic as a function of ICP power and pressure are compared to measurements using conventional N_2 OES and TDLAS to establish its feasibility and accuracy.

In the second part of this paper, we use the most appropriate gas temperature diagnostic, N_2 OES in this case, to investigate the temporal evolution of rotational temperature in a pulsed O_2 ICP plasma. The use of power-modulation, or pulsing, of plasmas limits the time-averaged power deposition, and therefore gas temperature, but maintains high plasma densities during the plasma pulse. It therefore offers an independent control over the electron temperature and gas temperature of the plasma, both of which are important for the plasma chemistry of the discharge.[7] In addition, power-modulation allows treatment of heat-sensitive materials, for example plastics, with high-power, high-density plasma processes.[8] In practice, plasma pulsing

introduces transient effects when the plasma is switched on, or off,[9–11] which are not fully understood, making pulse optimization often an empirical process. Temporal evolution of electron properties is regularly reported, e.g.[9–11] however, evolution of gas temperature during a plasma pulse is not often studied or taken into account in modeling.[12,13] Duten et al. reports gas temperature measurements in a pulsed, medium pressure microwave discharge in hydrogen,[7] while Macko and Veis measured gas temperatures in a pulsed glow discharge in oxygen.[14] We measure the temporal evolution of gas temperature in a plasma pulse with the aim to inform decisions about pulse duration for a desired gas temperature as well as investigate plasma formation mechanisms in a pulsed ICP.

2. Experimental methods

First, we describe the plasma system under study, then we will describe the different diagnostics that were used to measure the (time-resolved) rotational and translational temperatures of the plasma.

2.1. Experimental arrangement

The plasma under study here is an inductive version of the GEC reference cell,[15] with a 100 mm diameter grounded bottom electrode, and a powered top electrode consisting of a water-cooled three-turn double-spiral copper coil inside a 140 mm diameter quartz glass cylinder flange of about 7 mm wall thickness, which separates the coil from the plasma. The discharge gap is 40 mm. A turbomolecular pump achieved a base pressure of less than 10^{-5} Pa. During plasma operation a scroll pump adjusted the pressure between 20 and 50 Pa of pure oxygen (with optional admixtures for diagnostic purposes as described later). Gas is supplied to the chamber using thermal mass flow controllers, operating in the range 5–20 sccm. Gas pressure is set by manually adjusting the admitted gas flow (5–20 sccm) and adjustable valve towards the pumping system. There is no real-time control of the gas pressure. The applied RF power is between 100 and 900 W. The driving frequency was 13.56 MHz and an L-type matching network was used for matching the effective load impedance to the RF generator impedance of 50 Ohm. The

© 2020 The Japan Society of Applied Physics

RF power is applied to the central connection of the coil, with the opposite end of the coil grounded. For all pressures, the E-H mode transition, i.e. a transition between a capacitively coupled electron heating mode and an inductively coupled heating mode,[16,17] occurs within this power range.

The TDLAS diagnostic consists of a narrowband (100 kHz) tunable diode laser (Toptica Photonics DL Pro) that operates around 810.4 nm. A beam splitter directs 10% of the beam to a confocal Fabry–Perot interferometer (Thorlabs SA200-8B) with a free spectral range of 1.5 GHz. The transmitted light is detected by a photodiode, connected to an oscilloscope, for laser wavelength calibration. The main laser beam is attenuated by a neutral density filter (OD 4.5) to avoid saturation broadening of the absorbing transition, before it enters the plasma vessel through an anti-reflection-coated optical window. The transmitted beam is detected on the opposite side of the vessel, using a fast (14 ns rise time), biased Si photodiode (Thorlabs DET36A/M), with an interference filter to isolate the laser wavelength from the plasma and background light.

For the OES diagnostics, an optical fibre is positioned at the quartz window of the vacuum system, approximately 300 mm from the plasma centre. Light from the entire plasma volume is collected by the fibre. This light then enters a Czerny–Turner spectrometer (Andor Shamrock 500i), coupled to an intensified charge couple device (ICCD) camera (Andor iStar 334T). A grating with 1200 lines mm^{-1} is used giving a spectral window of about 40 nm detected on the ICCD with a resolution of 300 pm (instrumental broadening). The full experimental setup, including diagnostics is schematically shown in Fig. 1.

2.2. OES of the $O_2(b^1\Sigma_g^+)$ to $O_2(X^3\Sigma_g^-)$ band

The rotational band of interest is from the low-lying, long-lived $O_2(b, v' = 0)$ state to the ground state of oxygen, $O_2(X, v'' = 0)$:

$$O_2(b^1\Sigma_g^+, v' = 0) \rightarrow O_2(X^3\Sigma_g^-, v'' = 0). \quad (1)$$

It is an allowed magnetic dipole transition, resulting in the 4 rotational branches, ^RR, ^RQ, ^PP, ^PQ.

This specific transition was first described from its detection in stellar and atmospheric physics in 1961,[18] and since has been used for the determination of gas temperatures in DC glow discharges through OES, in some cases down to pressures of 70 Pa (0.5 Torr).[5,19,20] It has only recently been applied to a low-pressure RF ICP in the work of Wegner et al.[21] where measurements between 1 and 35 Pa were taken, however the technique used there was microwave interferometry, and not passive OES as utilised here.

The intensity I of an individual J' to J'' line of the rotational band is given by:

$$I_{J''}^{J'} = CS_{J''}^{J'} \exp\left(\frac{-F_{J'}hc}{k_B T_{rot}}\right), \quad (2)$$

where:

$$F_{J'} = B_{v'=0}J'(J'+1) - D_{v'=0}(J'(J'+1)^2) \quad (3)$$

is the term energy of the upper state, and J', J'' are the rotational quantum number of the upper and lower level respectively, C a proportionality factor, h Planck's constant, c the speed of light, k_B Boltzmann's constant, $B_{v'=0}$ and $D_{v'=0}$ the rotational constants of the upper state of 1.391 38 cm^{-1} and $5.486 \times 10^6 cm^{-1}$ respectively, and T_{rot} the rotational temperature of the molecule. The factor $S_{J''}^{J'}$ in the equation above is the Höln–London factor.[22] Our simulation of line positions and intensities as a function of the gas temperature is based on the scheme described in[18] and data stated in the references within. An assumption is made that the population distribution in the upper state is that of the lower state, and
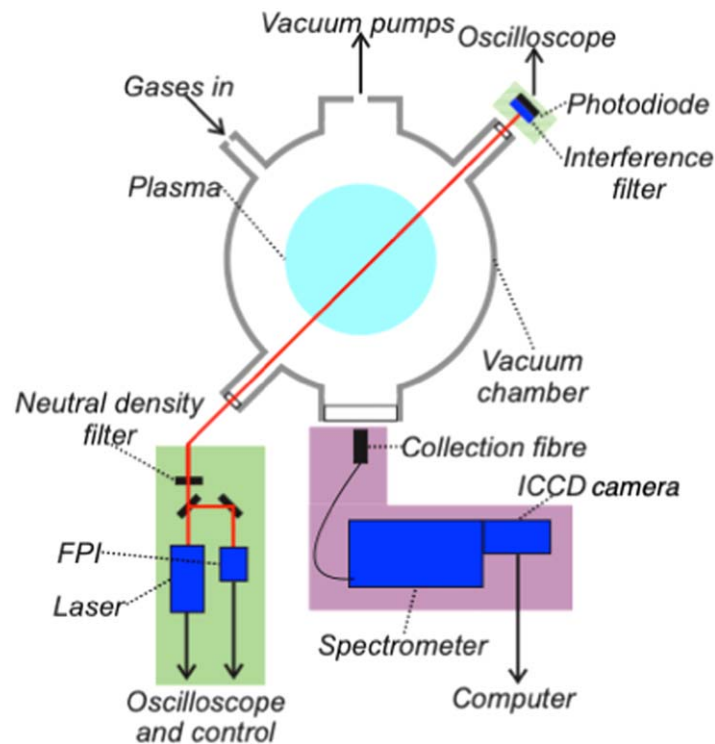

Fig. 1. (Color online) Top down view of the plasma system and the diagnostic set-ups used. Components highlighted in green are for tunable diode laser absorption spectroscopy. FPI is a Fabry–Perot interferometer. Components highlighted in pink are for optical emission spectroscopy.
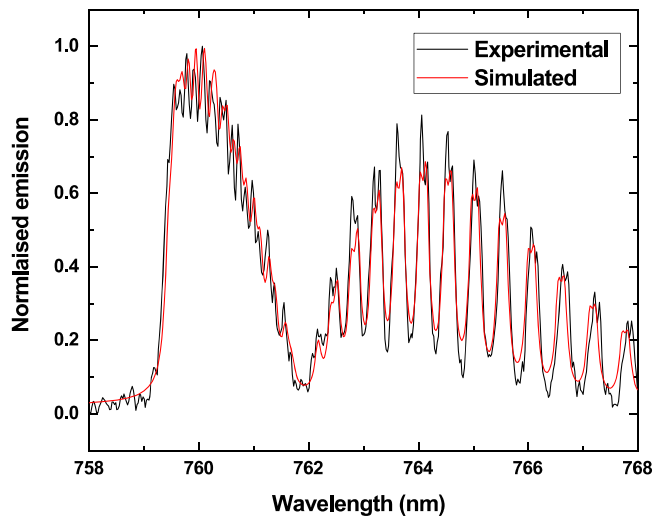
Fig. 2. (Color online) Fitted simulated and experimental spectra for $O_2(b^1\Sigma_g^+)$ to $O_2(X^3\Sigma_g^-)$ band from a 50 Pa, 300 W plasma in O_2. The resulting rotational temperature was 528 ± 15 K. The error estimate represents the standard deviation (of the fitting parameter) within the nonlinear least square fitting procedure used to match simulated spectrum to the measurement.

Fig. 3. (Color online) Fitted simulated and experimental spectra for $N_2(C^3\Pi_u)$ to $N_2(B^3\Pi_g)$ band from a 50 Pa, 300 W plasma in O_2 with 10% N_2 admixture. The resulting rotational temperature was 561 ± 20 K. The error estimate represents the standard deviation (of the fitting parameter) within the nonlinear least square fitting procedure used to match simulated spectrum to the measurement.

described by a Boltzmann distribution, which requires a sufficient number of collisions between molecules for this to occur.

In order to derive a temperature from experimental spectra, they are fitted with modelled spectra, with the temperature T_{rot} as a fitting parameter. It was found that there was a slight discrepancy between the positions of the experimental and modelled peaks. In particular, the gap between the RQ, RR and PQ, PP branches was not reproduced accurately in the model. This is most likely due to inaccuracies in the calculation of the level energies [Eq. (3)] and in particular the values for the rotational constants. A compression of the wavelength scale of the model by 2% around 762 nm was applied to match the positions of the modelled spectrum to the experimental ones. The result is a good fit between measurement and simulation and the associated value for T_{rot} can be interpreted as reasonably accurate. Figure 2 shows an example of a measured and modelled spectrum.

2.3. Optical emissions spectroscopy of the $N_2(C^3\Pi_u)$ to $N_2(B^3\Pi_g)$ band

The molecular transition of interest here is the $N_2(C)$ to $N_2(B)$ transition, also known as the second positive system. In particular we focus on the band:

$$N_2(C^3\Pi_u, v' = 0) \rightarrow N_2(B^3\Pi_g, v'' = 0). \tag{5}$$
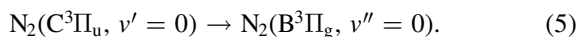
This transition is widely used for determining rotational temperatures in plasmas. The main idea is the same as for the O_2 OES method; theoretical spectra with T_{rot} as a fitting parameter are fitted to experimental spectra to derive the rotational temperature. A recent review by Bruggeman et al.[4] discusses the theoretical background in more detail. In addition, a detailed description of the model describing this transition can be found in.[23,24]

For our case, the use of N_2 OES does mean that an admixture of N_2 needs to be added to our O_2 plasma. An admixture of 10% was used, which had negligible effect on the rotational temperatures of the plasma. i.e. rotational temperatures determined by O_2 OES gave the same value
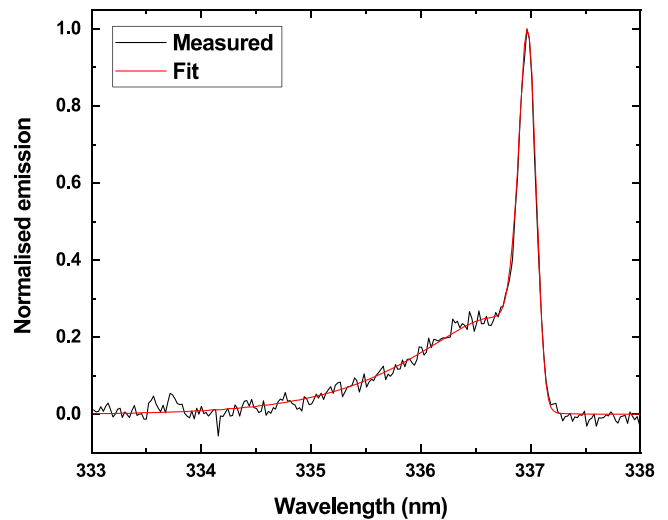
for pure O_2 and O_2 with 10% N_2 plasmas. Of course, a 10% N_2 admixture will certainly change other properties of the plasma significantly, e.g. plasma chemistry, making it unsuitable for in situ monitoring in industrial processing conditions. However, in this paper we only use N_2 OES to measure rotational gas temperature to compare with O_2 OES measurements and to study the fundamental plasma physics of gas heating during a plasma pulse. For both these studies, the N_2 admixture has negligible influence on the measured plasma parameters. Figure 3 shows an example of a measured and fitted simulated spectra for a 50 Pa, 300 W plasma in O_2 with 10% N_2.

2.4. TDLAS on the $Ar(1s_4)$ resonant state

TDLAS is another well-established technique for measuring gas temperatures in low-temperature plasmas.[25–27] Typically, visible or near-infrared tunable diode lasers are used to detect transitions in argon or helium atoms in the plasma, either as working gas or as admixture. In our case, we investigated absorption from a resonant state of argon instead of the more commonly used metastable state. Tian et al.[28] have shown in modelling that the resonant state has a density about an order of magnitude lower than the metastable state under low-pressure conditions. Our laser operates around 810.4 nm, corresponding to the transition $Ar (1s_4) \Rightarrow Ar (2p_7)$. An admixture of 15% Ar in O_2 is used for all measurements in this paper. The value of 15% was chosen as the minimum value needed to perform TDLAS measurements under all plasma conditions. Again, it is likely that the plasma chemistry of the discharge will be affected by this admixture, however we only measure the gas temperature which is not affected much. i.e. rotational temperatures determined by O_2 OES gave the same value for pure O_2 and O_2 with 15% Ar plasmas. This is in line with measurements by Wegner et al.[29] of ion saturation current, line-integrated electron density and E-H mode transition voltages for a range of Ar/O_2 mixtures in a 10 Pa ICP. For pure O_2 and 25% Ar, the values are within roughly 10% of each other, giving some confidence that also the gas temperature is minimally affected by the admixture.
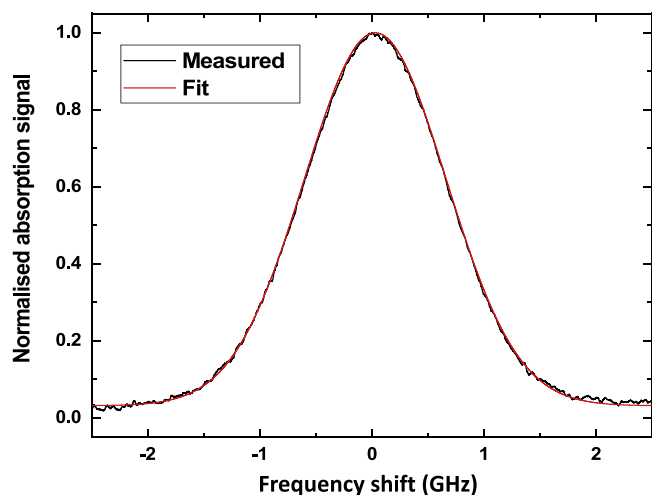
Fig. 4. (Color online) Fitted and experimental spectra for laser absorption around 810.4 nm (Ar($1s_4$) $\Rightarrow$ Ar($2p_7$) transition) obtained with tunable diode laser absorption spectroscopy in a 50 Pa, 600 W O_2 discharge with 15% Ar. The resulting translational temperature calculated from a FHWM of Doppler broadening was 1600 ± 190 K.

The translational temperature of the plasma is determined from the Doppler broadening of the absorption transition. Other broadening mechanisms are negligible under these conditions. That is, pressure broadening can be estimated to be in the range 1.9–10 MHz for temperatures 300–1600 K, using the self-broadening data for this transition from Tachibana et al.[30] Broadening by other species in the plasma can be larger, nevertheless, it will be much less than the Doppler broadening which is in the order of 1 GHz. As discussed before, saturation broadening is avoided by including sufficient neutral density filtering. A Gaussian function is fit to the experimental data to determine the Doppler width, from which the gas temperature is derived. An example of an observed TDLAS signal and a fitted function is shown in Fig. 4.

3.   Results and discussion

3.1.   Comparison of diagnostics
Figure 5 shows the results of translational and rotational temperature measurements using the three diagnostic techniques as a function of plasma power (100–900 W) for pressures of 20 and 50 Pa. The plasma was run in continuous mode for these measurements.

The first consideration to make is whether the rotational temperatures (measured by N_2 and O_2 OES) can be expected to be in equilibrium with the translational (gas) temperatures (TDLAS). Bruggeman et al.[4] conclude that as long as the main population mechanism for the excited state is direct electron impact from the ground state, the rotational temperature is a good estimate for the translational (gas) temperature. This includes N_2 OES for most plasmas, as long as they do not contain Ar (due to N_2(C) production from Ar* collisions). For O_2 OES this will be the case for low-density plasmas, but for higher densities, significant population of the O_2($b^1\Sigma^+_g$) state through electronic excitation transfer from metastable O(^{1}D) atoms will become important, which can prohibit the equilibrium between rotational and translational temperatures.[31]

The sharp increase in temperature observed at 425 W for 50 Pa is associated with the E to H mode transition in the plasma. Visual inspection confirmed a mode change at these powers, as shown in Fig. 6.

For 20 Pa, there is a similar, but less pronounced step at about 250 W. This is likely to be a transition from E-mode to an E/H hybrid mode, as identified by Wegner et al.[21] for plasmas below 30 Pa. It is not clear from these measurements whether there is the transition into full H-mode for high powers.

Across the E to H mode transition, a sharp increase in electron density is expected, which leads to an increase in dissociation of O_2, releasing thermal energy and increasing gas temperature, as observed in.[21,32] In addition, the gas temperature is relatively insensitive to the gas pressure, similar to the observations of Wegner et al. for electron density for varying gas pressures.[21]

When comparing the different diagnostic techniques, the first thing to note is that for E-mode plasmas, all three diagnostics agree well with each other. The exception is Ar TDLAS for the 50 Pa case, where no measurements could be made due to a lack of absorption signal. This is believed to be caused by significant depopulation of the Ar ($1s_4$) state by dissociation and Penning ionisation reactions with O_2, as discussed by Takechi and Lieberman[33] for similar Ar/O_2 plasmas. Wegner et al. show that for H-mode the O_2 ground state density decreases compared to E-mode, as a result of increased electron impact dissociation (increased O density).[21] Similar, for decreasing pressure, the O_2 density decreases for all plasma powers (both E-mode and H-mode).[21,33] Therefore, for both H-mode at 50 Pa and all measurements at 20 Pa, there is a lower density of O_2 in the plasma, compared to 50 Pa E-mode, and therefore a reduction in the reaction rates between Ar($1s_4$) and O_2, leading to a higher density of Ar($1s_4$), allowing reliable TDLAS measurements for these conditions.

For H-mode operation Ar TDLAS and N_2 OES agree well, within 5%–10%, for all powers. The O_2 OES diagnostic only gave measurable results for relatively low powers (300–400 W at 20 Pa and 500–600 for 50 Pa). However, these were not in agreement with the other two diagnostics. The most likely reason for this is that in H-mode, there is a significant increase in O_2 dissociation by electrons, leading to a higher atomic oxygen density.[21,32] This in turn means that there will be a significantly higher density of the metastable O(^{1}D) atoms, which can populate the O_2(b) state:[31]

$$O(^1D) + O_2(X^3\Sigma_g) \Rightarrow O_2(b^1\Sigma_g) + O(^3P).$$
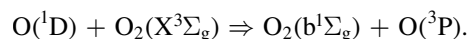
The metastable O(1D) atoms are mainly produced by electron impact dissociation of O_2 which means their temperature is not in equilibrium with the gas temperature, resulting in a non-equilibrium rotational distribution of the O_2(b) state, resulting in the O_2 OES rotational temperature fits deviating from the other two diagnostics.

In addition, the O_2 OES diagnostic did not provide any measurable results for high powers (>400 W for 20 Pa, >600 W for 50 Pa), due to a reduction of the observed emission signal. Reason for this is that the upper state, O_2(b), is believed to be heavily quenched by ground state atomic oxygen:[31,34,35]
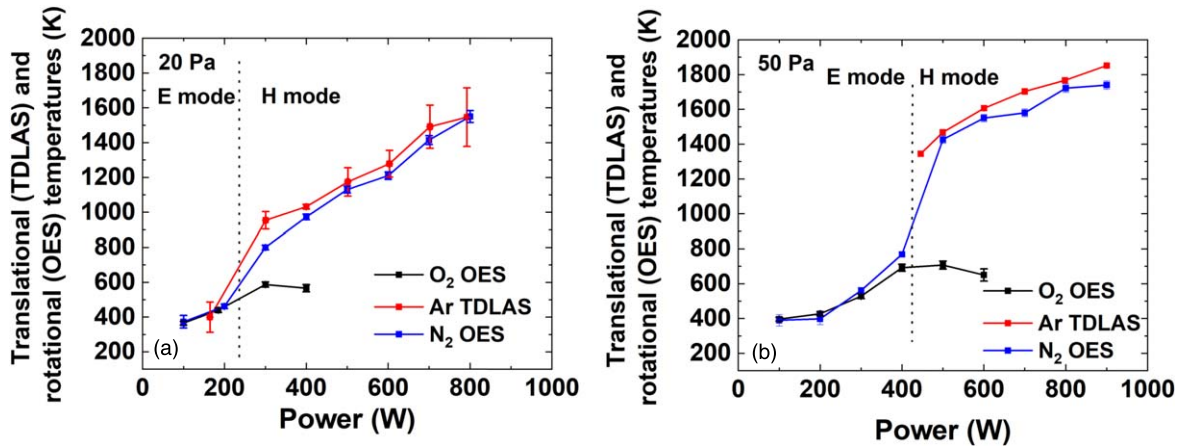
Fig. 5. (Color online) Translational (TDLAS) and rotational (OES) temperature as a function of power for pressures of 20 (a) and 50 Pa (b), measured using three diagnostic techniques (O$_2$ OES, N$_2$ OES, Ar TDLAS). The vertical dashed lines indicate the observed E to H mode transition of the ICP.

Fig. 6. (Color online) Left: ICP plasma operating in E-mode (50 Pa, 400 W). Right: ICP plasma operating in H-mode (50 Pa, 500 W).

$$O_2(b^1\Sigma_g) + O(^3P) \Rightarrow O_2(a^1\Delta_g) + O(^3P).$$
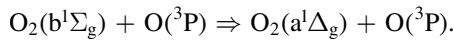
Nevertheless, Fig. 6 shows that O$_2$ OES can provide accurate gas temperature measurements in low-density (E-mode) O$_2$ plasmas, in agreement with well-established techniques such as N$_2$ OES and Ar TDLAS. Of course, many industrial processing applications work at high densities, i.e. H-mode, for which this diagnostic is not suitable, limiting its industrial applicability to specific low-density applications.

3.2. Time-solved investigation of gas heating in a pulsed ICP
In addition, gas heating during pulsed operation of the ICP was studied using N$_2$ OES. This diagnostic was chosen because it works well across all pressures and powers of interest (see Fig. 5) and it can provide adequate time-resolution. The natural lifetime of the upper N$_2$(C$^3\Pi_u$, $v' = 0$) state is 36.6 ns,[36] and the measurement time is 200 μs. Achieving adequate time-resolution with TDLAS is more complex since a complete wavelength sweep takes longer than 200 μs, so partial acquisition over multiple pulses would be needed, making N$_2$ OES a more suitable choice.

Figure 7 shows the temporal evolution of the rotational temperatures during a 30 ms plasma pulse in a 5 Hz pulsed ICP.

The measurements were performed using an ICCD gate time of 200 μs, while the delay between the start of the plasma pulse and the ICCD gate was varied. Light from multiple plasma pulses was accumulated. Depending on the intensity of the light emitted during the gate interval, between 75 and 500 plasma pulses were integrated to obtain good signal-to-noise. Four plasma cases were investigated, 20 Pa at both 500 and 700 W RF power and 50 Pa at 700 W. For the 50 Pa, 700 W case, the measurement was repeated on a different day, re-optimising the matchbox settings (labelled as "50 Pa 700 W repeat" in Fig. 7). It should be noted that for both cases, good matching was achieved with <0.3% reflected power.

Figure 7 shows that for all cases there is a rapid increase in temperature, taking about 1–3 ms, after which it is relatively constant. The difference is that for three of the cases (20 Pa both powers and one of the 50 Pa, 700 W cases), this increase happens right at the start of the pulse, while for the "50 Pa, 700 W repeat" case, there is a delay of about 4 ms before the increase happens. The transition time of 1–3 ms is slightly longer than what is typically reported in literature after a change in power, or start of a plasma pulse. In most situations, the plasma reaches steady-state operation in about 0.5–1 ms.[9–11] However, this is likely due to the low duty cycle (15%) and repetition rate (5 Hz), compared to the experiments in literature. This means that in our case, during the off-time the electron density drops more significantly, requiring a longer "ignition phase" during which the electron density builds up again at the start of the next pulse.

Comparing the 20 Pa cases, we notice that the 700 W case has a more rapid increase in rotational temperature compared to the 500 W case. This can be explained by the fact that higher power will lead to a more rapidly increasing electron
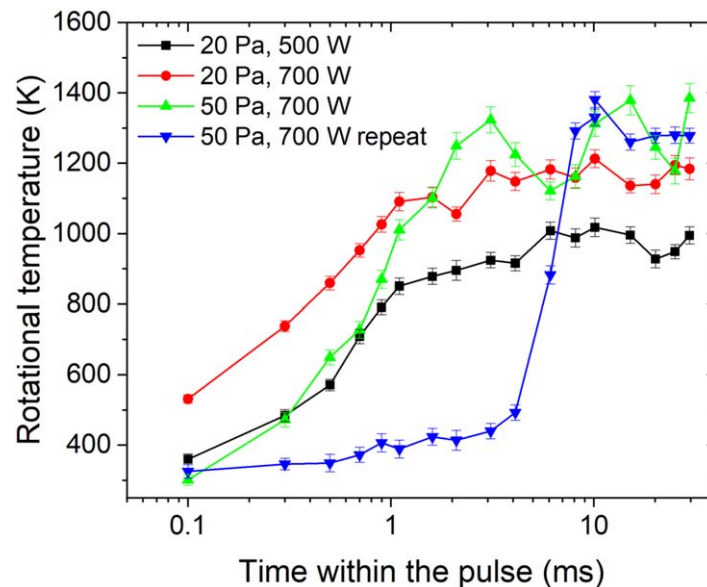
Fig. 7. (Color online) Rotational temperature measurements within a plasma pulse, measured with the N_2 OES diagnostic technique. The plasma was an O_2 ICP with 10% N_2 admixture. Pressures of 20 Pa (500 and 700 W RF power) and 50 Pa (700 W RF power) were investigated. ICCD gate time was 200 μs with the delay between the ICCD gate and the start of the plasma pulse varied. Points in the graph represent the middle of the ICCD gate time, e.g. 0.1 ms is a gate time of 0–0.2 ms.

density and therefore rotational temperature. Also, in steady-state, i.e. after $\sim$5–10 ms, the 700 W case will have a higher rotational temperature due to the higher electron density compared to the 500 W case.

Comparing the 700 W cases, i.e. 20 and 50 Pa (red dots and green upright triangle in Fig. 7), we can see that the rotational temperature for 20 Pa is higher than for 50 Pa during the temperature rise. Brockhaus et al.[9] established through modelling that during the ignition phase, the electron density decreases with increasing pressure. Here, the higher electron density for 20 Pa leads to higher rotational temperatures during the ignition phase.

Because electron density will reduce significantly during the off-period, ignition of the next pulse will not be in H mode, it has to start up in capacitive or E mode. The power supply and matching network will therefore also play a significant role in the plasma ignition since the matching network settings are fixed and optimised for inductive mode, which means that the capacitive power coupling is not optimal. Depending on the exact settings of the matching network, this could be a significant effect, see for example the "50 Pa, 700 W repeat" case in Fig. 7. Here, the matching settings turn out to be such that there is limited power deposition and a much slower plasma development. This effect can be amplified by the power supply output level regulation, i.e. if there is high reflected power, the forward power will be limited for safety reasons. This power regulation typically works on a timescale of $\sim$1–10 ms for our power supply. Eventually, after about 4 ms, there is sufficient plasma to trigger an E to H mode transition. Since with increasing inductive mode contributions, the power coupling efficiency increases (since this was optimized for H mode) and electron density rapidly increases and a H mode is established. It should be noted that there was no visual difference between the two 50 Pa, 700 W cases and matching was good with <0.3% reflected power for both cases. It is only when time-resolved plasma parameters, such as rotational temperature, are measured it becomes clear that

there is a significant difference between the two cases. This means that for short pulses (at low duty cycles), typically less than about 10 ms, the power supply and matching network will need to be considered and monitored carefully to enable reliable operation of the pulsed plasma.

One thing that is not explicitly clear from these measurements is whether the rotational and gas temperatures follow changes in the electron density immediately or whether there is a delay between the two. However, times between collisions for electrons and neutrals under our conditions are typically less than 1 μs, which means that on the timescales of $\sim$100 μs investigated here, it is likely that the rotational and gas temperatures have adjusted themselves to changes in electron density. Time-resolved measurements of electron density would be needed to determine exactly how much delay there is between a change in electron density and a change in rotational and gas temperatures.

4. Conclusions

First, the feasibility of using a magnetic dipole transition in molecular oxygen as a non-intrusive gas temperature diagnostic for oxygen plasmas was investigated. Measurements were compared to more standard techniques requiring admixtures for diagnostic purposes. i.e. N_2 OES on the $N_2(C)$ to $N_2(B)$ transition and TDLAS of the $Ar(1s_4) \Rightarrow Ar(2p_7)$ transition. It was found that O_2 OES can provide accurate gas temperature measurements in low-density (E-mode) O_2 plasmas, making it an appealing option for gas temperature monitoring for these types of discharges. For high-density (H-mode) operation at high powers, the O_2 OES did not provide accurate measurements, most likely due to non-equilibrium population of the $O_2(b)$ state by metastable atomic oxygen (O^1D).

Second, the gas temperatures measured range from about 400 K in low-power E-mode to over 1800 K for high-power H-mode. A rapid increase in gas temperature is associated with the E to H mode transition that is observed for

increasing power. An increasing electron density with power leads to an increase in dissociation of O_2, releasing thermal energy and increasing gas temperature.

In pulsed operation at low duty cycles, it takes about 1–3 ms before the steady-state gas temperatures are achieved. This is slightly longer than the transition time of $\sim$0.5–1 ms that can be observed for pulsed plasmas with higher duty cycles.[9–11] The difference due to a longer afterglow period and therefore lower electron density at the start of the pulse. Rotational temperatures during the first 1–2 ms are found to be higher for higher powers (at the same pressure) and lower pressure (at the same power), both of which are in line with electron density trends during plasma ignition.[9]

Finally, it was observed that the power supply output regulation and matching network settings can have a significant effect on the plasma ignition of a pulsed plasma. An ignition delay of up to 4 ms was observed for 50 Pa, 700 W with different matching network settings, but with the same 'match quality' ($<$0.3% reflected power). It can therefore be concluded that for short pulses, less than about 10 ms, the power supply and matching network will need to be carefully monitored and optimised to enable reliable operation of a pulsed ICP in oxygen.

Acknowledgments

ORCID iDs

Erik Wagenaars https://orcid.org/0000-0002-5493-3434

1) J. Hopwood, Plasma Sources Sci. Technol. **1**, 109 (1992).
2) A. R. Gibson, M. Foucher, D. Marinov, P. Chabert, T. Gans, M. J. Kushner, and J.-P. Booth, Plasma Phys. Control. Fusion **59**, 024004 (2017).
3) S. Reuter, J. Santos Sousa, G. D. Stancu, and J. P. H. van Helden, Plasma Sources Sci. Technol. **24**, 054001 (2015).
4) P. J. Bruggeman, N. Sadeghi, D. C. Schram, and V. Linss, Plasma Sources Sci. Technol. **23**, 023001 (2014).
5) S. M. Zyryanov and D. V. Lopaev, Plasma Phys. Rep. **33**, 510 (2007).
6) D. N. Meehan and E. Wagenaars, Proc. Int. Conf. Phenomena in Ionized Gases (ICPIG), 2019 OR19AM-B01.
7) X. Duten, A. Rousseau, A. Gicquel, K. Hassouni, and P. Leprinc, J. Phys. D: Appl. Phys. **35**, 1939 (2002).
8) S. Rajendiran, A. K. Rossall, A. Gibson, and E. Wagenaars, Surf. Coat. Technol. **260**, 417 (2014).
9) A. Brockhaus, G. F. Leu, V. Selenin, K. Tarnev, and J. Engemann, Plasma Sources Sci. Technol. **15**, 171 (2006).
10) F.-X. Liu, T. V. Tsankov, and Y.-K. Pu, J. Phys. D: Appl. Phys. **48**, 035206 (2015).
11) T. List, T. Ma, P. Arora, V. M. Donnelly, and S. Shannon, Plasma Sources Sci. Technol. **28**, 025005 (2019).
12) M. A. Lieberman and S. Ashida, Plasma Sources Sci. Technol. **5**, 145 (1996).
13) B. Ramamurthi and D. J. Economou, Plasma Sources Sci. Technol. **11**, 324 (2002).
14) P. Macko and P. Veis, J. Phys. D: Appl. Phys. **32**, 246 (1999).
15) P. A. Miller and G. A. Hebner, J. Res. Natl. Inst. Stand. Technol. **100**, 427 (1995).
16) U. Kortshagen, N. D. Gibson, and J. E. Lawler, J. Phys. D: Appl. Phys. **29**, 1224 (1996).
17) K. A. MacKinnon, Phil. Mag. **8**, 605 (1929).
18) J. Noxon, Can. J. Phys. **39**, 1110 (1961).
19) M. Touzeau, M. Vialle, A. Zellagui, G. Gousset, M. Lefebvre, and M. Pealat, J. Phys. D: Appl. Phys. **24**, 41 (1991).
20) P. Veis and G. Cernogora, Czech. J. Phys. **48**, 75 (1998).
21) T. Wegner, C. Küllig, and J. Meichsner, Plasma Sources Sci. Technol. **26**, 025006 (2017).
22) G. Herzberg, Molecular Structure and Molecular Spectra I. Spectra of Diatomic Molecules (Van Nostrand, New York, 1950).
23) I. Kovacs, Astrophys. J. **145**, 634 (1966).
24) A. Schadee, Astron. Astrophys. **41**, 203 (1975).
25) D. O'Connell, T. Gans, D. Crintea, U. Czarnetzki, and N. Sadeghi, J. Phys. D: Appl. Phys. **41**, 035208 (2008).
26) S. Schröter, H. Bahre, M. Böke, and J. Winter, Plasma Process. Polym. **11**, 239 (2014).
27) B. Clarenbach, B. Lorenz, M. Krämer, and N. Sadeghi, Plasma Sources Sci. Technol. **12**, 345 (2003).
28) P. Tian and M. J. Kushner, Plasma Sources Sci. Technol. **26**, 024005 (2017).
29) T. Wegner, C. Küllig, and J. Meichsner, Contrib. Plasma Phys. **55**, 728 (2015).
30) K. Tachibana, H. Harima, and Y. Urano, J. Phys. B: At. Mol. Phys. **15**, 3169 (1982).
31) O. Braginskiy, A. Vasilieva, K. Klopovskiy, A. Kovalev, D. Lopaev, O. Proshina, T. Rakhimova, and A. Rakhimov, J. Phys. D: Appl. Phys. **38**, 3609 (2005).
32) R. Zaplotnik, A. Vesel, and M. Mozetic, Europhys. Lett. **95**, 55001 (2011).
33) K. Takechi and M. A. Lieberman, J. Appl. Phys. **90**, 3205 (2001).
34) I. Kossyi, A. Y. Kostinsky, A. Matveyev, and V. Silakov, Plasma Sources Sci. Technol. **1**, 207 (1992).
35) T. Slanger and G. Black, J. Chem. Phys. **70**, 3434 (1979).
36) K. Becker, H. Engels, and T. Tatarczyk, Chem. Phys. Lett. **51**, 111 (1977).